AGU PUBLICATIONS

Geophysical Research Letters

RESEARCH LETTER
10.1002/2015GL065005

Special Section:
First Results from the MAVEN Mission to Mars

Marsward and tailward ions in the near-Mars magnetotail: MAVEN observations

Y. Harada[1], J. S. Halekas[2], J. P. McFadden[1], D. L. Mitchell[1], C. Mazelle[3,4], J. E. P. Connerney[5], J. Espley[5], D. E. Larson[1], D. A. Brain[6], G. A. DiBraccio[5], S. M. Curry[1], T. Hara[1], R. Livi[1], S. Ruhunusiri[2], and B. M. Jakosky[6]

[1]Space Sciences Laboratory, University of California, Berkeley, California, USA, [2]Department of Physics and Astronomy, University of Iowa, Iowa City, Iowa, USA, [3]IRAP, CNRS, Toulouse, France, [4]Paul Sabatier University, Toulouse, France, [5]NASA Goddard Space Flight Center, Greenbelt, Maryland, USA, [6]Laboratory for Atmospheric and Space Physics, University of Colorado Boulder, Boulder, Colorado, USA

Abstract We present Mars Atmosphere and Volatile EvolutioN (MAVEN) observations of Marsward and tailward fluxes of suprathermal (>25 eV) ions in the near-Mars (~1–1.5 Mars radii downstream) magnetotail. Statistical results show that the Marsward proton flux and magnetic field draping pattern are well organized by the upstream motional electric field direction. We observe both significant Marsward proton fluxes and tightly wrapped magnetic field lines in the hemisphere pointed in the opposite direction to the upstream electric field. These characteristics are very similar to those observed at Venus. On the other hand, the net flux of oxygen ions points tailward on average in the Martian tail, while net Venusward flows of oxygen ions were observed frequently in the same hemisphere at Venus. The mechanism by which the Marsward proton flux is produced in the presence of tailward oxygen ion flux remains unclear.

Key Points:
- Ions and magnetic fields in the near-Mars tail are organized by the upstream electric field
- Marsward protons and wrapped field lines are observed in the $-E$ hemisphere
- Unlike at Venus, net flux directions differ between protons and oxygen ions at Mars

Correspondence to:
Y. Harada,
haraday@ssl.berkeley.edu

Citation:
Harada, Y., et al. (2015), Marsward and tailward ions in the near-Mars magnetotail: MAVEN observations, *Geophys. Res. Lett.*, *42*, doi:10.1002/2015GL065005.

Received 18 JUN 2015
Accepted 2 AUG 2015

1. Introduction

The solar wind interaction with an unmagnetized body with a significant atmosphere leads to the formation of an induced magnetosphere [*Nagy et al.*, 2004]. As the solar wind flow is slowed down because of mass loading and the interplanetary magnetic field (IMF) cannot be readily diffused into the conductive ionosphere, the IMF piles up on the dayside and drapes around the obstacle. The draped IMF is stretched downstream by the supersonic solar wind flow, forming a long tail on the nightside. The nightside magnetotail consists of the tail lobes with dominantly sunward and antisunward magnetic fields separated by the plasma sheet, the orientation of which is controlled by the upstream IMF direction.

As the magnetotail plasma sheet provides one of the main pathways of escaping planetary ions [*Brain et al.*, 2010], ion fluxes in the Martian and Venusian magnetotails have been extensively studied [see, e.g., *Dubinin et al.*, 2012a, and references therein]. The solar wind interactions with Mars and Venus are similar in terms of the formation of induced magnetospheres, but they also have differences such as gravity, crustal field strengths, and solar wind conditions. Tailward fluxes of planetary ions in the Martian and Venusian tails are associated with escape fluxes from the planetary ionosphere/exosphere. The tailward ion fluxes are strongly correlated with the upstream solar wind dynamic pressure [*Lundin et al.*, 2008], and their spatial distributions are well organized by the IMF direction [*Slavin et al.*, 1989; *Barabash et al.*, 2007; *Fedorov et al.*, 2008]. On the other hand, Venus Express observations have revealed the presence of planetward (sunward) ion flows at Venus [*Lundin*, 2011; *Zhang et al.*, 2012; *Dubinin et al.*, 2012b, 2013]. Such Venusward/return flows are primarily observed in the hemisphere pointed in the opposite direction to the motional electric field in the upstream solar wind (so-called "$-E$ hemisphere"). This hemispheric asymmetry of Venusward ions has been associated with the asymmetric magnetic field draping pattern which shows field line wrapping in the $-E$ hemisphere [*Zhang et al.*, 2010; *Du et al.*, 2013; *Rong et al.*, 2014].

In this paper, we investigate Marsward and tailward ion fluxes in the near-Mars magnetotail (~1–1.5 R_M downstream), utilizing plasma and field measurements from the Solar Wind Electron Analyzer (SWEA) [*Mitchell et al.*, 2014], Solar Wind Ion Analyzer (SWIA) [*Halekas et al.*, 2013], Supra-Thermal And Thermal Ion Composition (STATIC) [*McFadden et al.*, 2014], and Magnetometer (MAG) [*Connerney et al.*, 2015] instruments on board the Mars Atmosphere and Volatile EvolutioN (MAVEN) mission [*Jakosky et al.*, 2015]. These MAVEN measurements

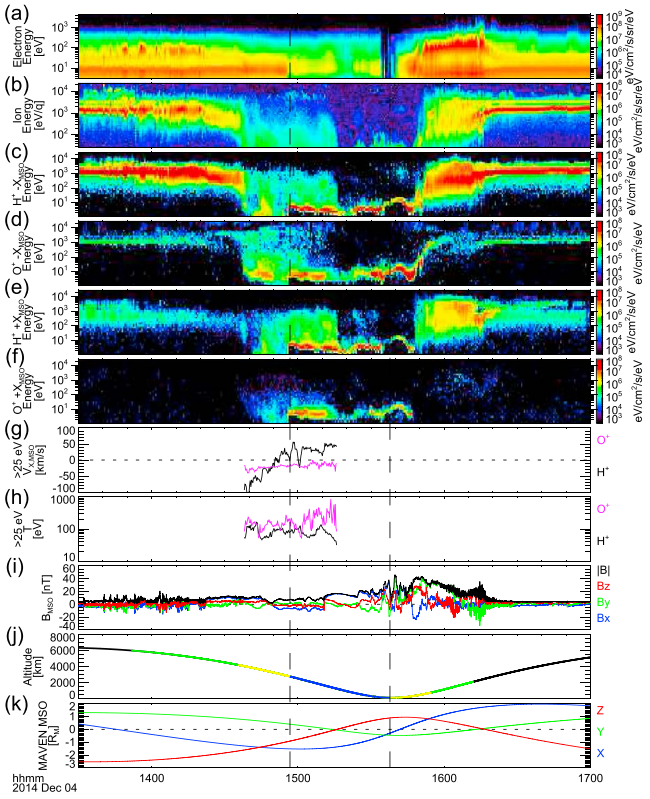

Figure 1. Time series of MAVEN observations of charged particles and magnetic fields on 4 December 2014. Energy-time spectrograms of (a) electrons from SWEA, (b) ions from SWIA, (c) antisunward protons, (d) antisunward oxygen ions, (e) sunward protons, (f) sunward oxygen ions, (g) X_{MSO} component of suprathermal (>25 eV) ion velocities, (h) temperatures of suprathermal ions from STATIC, (i) magnetic field in the MSO frame, (j) spacecraft altitude, and (k) spacecraft MSO position. The colors in the altitude plot in Figure 1j show the nominal regions, and the vertical dashed lines denote the wake boundaries (see text for detail).

provide us with the first comprehensive data sets of plasma and magnetic fields in the near-Mars magnetotail. The MAVEN observations reveal the net Marsward proton flux in the presence of net tailward oxygen ion flux in the near-Mars magnetotail, asymmetric distributions of the Marsward protons and IMF draping pattern relative to the upstream solar wind electric field direction, and the upstream dynamic-pressure control of the Marsward proton flux.

2. Case Study: 4 December 2014

We first present an example of MAVEN measurements to illustrate what ion populations contribute to the Marsward and tailward fluxes in the magnetotail. Figure 1 shows MAVEN data from a periapsis pass on 4 December 2014. In this time series, MAVEN starts from the solar wind, passes through the magnetosheath into the nightside magnetotail region in the inbound segment, penetrates through the ionosphere at the periapsis near the terminator, and exits the dayside ionosphere and magnetosheath in the outbound segment. The colors of the altitude plot in Figure 1j represent the nominal positions of the magnetosheath by green, the magnetic pileup region by yellow [*Trotignon et al.*, 2006], and the geometrical shadow by blue. Figure 1k shows the spacecraft location in the Mars Solar Orbital (MSO) frame, in which the *X* axis points from Mars toward the Sun, the *Y* points opposite to the direction of Mars' orbital velocity component perpendicular to *X*, and the *Z* completes the orthogonal coordinate set. The particle energy spectra and magnetic fields display typical signatures in each region: the solar wind is characterized by cold electrons and monoenergetic ion beams in weak magnetic fields; the magnetosheath is populated by heated plasma with turbulent magnetic fields; the magnetotail region contains both hot, tenuous plasma and cold, dense plasma in smoothly varying magnetic fields; and the low-altitude ionosphere is dominated by very cold plasma.

Here we focus on the ion populations in the magnetotail by looking at the angle-integrated, directional energy spectra of protons and oxygen ions (Figures 1c–1f). The directional energy flux is derived from angular integration of the differential energy flux multiplied by $\cos\theta$ for $\cos\theta > 0$ directions, where θ is the angle between the particle velocity and the direction of interest (i.e., sunward and antisunward). Figures 1c and 1d show the energy spectra of protons and oxygen ions traveling antisunward (tailward), while Figures 1e and 1f show those of ions traveling sunward (Marsward in the tail). The vertical dashed lines in Figure 1 denote the boundaries of the geometrical shadow ($\rho_{MSO} \equiv \sqrt{Y_{MSO}^2 + Z_{MSO}^2} < 1R_M$), which is defined as the Martian "wake" in this paper.

We note that we find several signatures related to the solar wind protons outside the wake. The monoenergetic line at ~1.5 keV seen before 14:22 and after 16:18 in the antisunward oxygen panel (Figure 1d) is due to contamination from solar wind proton stragglers, not oxygen signals. The broadband below ~1.5 keV in sunward protons during the same time intervals (Figure 1e) represents the protons backscattered from the spacecraft, not geophysical signals. Since this backscattered flux is typically 2 orders of magnitude smaller than the incoming flux, the backscattering contamination becomes negligible in the tail region. The ~1.5 keV signals of antisunward protons at 15:40–15:45 near the periapsis (Figure 1c) represent penetrating hydrogen atoms neutralized upstream of the bow shock and reionized in the ionosphere [*Halekas et al.*, 2015].

In the magnetotail region, we observe multiple populations of ions traveling tailward and Marsward. The tailward and Marsward proton spectra indicate the presence of hot protons with diffuse energy spectra at ~10–1500 eV (Figures 1c and 1e). These energy spectra suggest that the hot protons originate from the magnetosheath and ultimately from the solar wind, as pointed out regarding similar populations observed at Venus [*Lundin*, 2011; *Dubinin et al.*, 2013]. It is worth noting that the Marsward flux (Figure 1e) is larger than the tailward flux (Figure 1c) for these hot protons, indicating their net Marsward flux. In addition to this hot component, we observe the bright lines of cold protons below 10 eV (Figures 1c and 1e). The oxygen ion spectra exhibit the cold core populations below 10 eV and suprathermal tail populations extending up to ~100 eV (Figures 1d and 1f). The cold components of both hydrogen and oxygen ions are most likely supplied from the cold Martian ionosphere. The observed energies of these cold ions are determined primarily by the bulk velocity of the cold component in the spacecraft frame and by negative spacecraft potentials in shadow. The suprathermal tail populations of planetary ions could result from ion heating by ion-ion instabilities in the mixed plasma of magnetosheath and ionospheric origin [*Ergun et al.*, 2006; *Dubinin et al.*, 2013]. We also observe tailward oxygen ions with very high energies of ~5 keV (Figure 1d). These high-energy tailward oxygen ions should also originate from the planetary atmosphere/exosphere, but their energies well above the solar wind energy imply pickup acceleration from source locations outside of the wake [e.g., *Fang et al.*, 2008]. We note that the majority of the suprathermal and pickup oxygen ions travel tailward, though we do observe the Marsward flux of suprathermal oxygen ions as well (Figures 1d and 1f). Figures 1g and 1h show the $V_{x,MSO}$ and temperatures of protons and oxygen ions with energies above 25 eV. It is seen that the hot protons flow Marsward in the wake ($V_{x,MSO} > 0$), while the hot oxygen ions stream tailward ($V_{x,MSO} < 0$). The different net flux directions of protons and oxygen ions suggest kinetic or multifluid behavior of different ion species in the near-Mars magnetotail.

3. Statistical Results

In this section, we present statistical results using directional ion fluxes from STATIC measurements in the near-Mars magnetotail to investigate the dependence of the Marsward and tailward ions on the upstream and local parameters. Here we calculate upstream solar wind parameters (i.e., N_{SW}, $\mathbf{V}_{SW}$, and $\mathbf{B}_{SW}$) for each orbit from SWIA and MAG measurements in the solar wind. Then we linearly interpolate the two data points of two consecutive orbits to estimate upstream values in between. After discarding orbits with no available upstream parameters, we use total 438 orbits from 1 December 2014 to 28 February 2015. In this paper, we focus on ion fluxes of suprathermal components above 25 eV so that the spacecraft velocity and potential have negligible effects on the flux calculation. Nominal spacecraft velocities <4.5 km/s result in ram energies of <0.1 eV for protons and <1.7 eV for oxygen ions. The spacecraft potential typically floats around several volts negative in shadow, and its absolute value usually does not exceed 25 V in MAVEN orbits. The inclusion of low-energy ions will be addressed in future studies. Higher-energy ions above the STATIC energy limit ~30 keV are expected to be insignificant in terms of number flux within the near-Mars magnetotail.

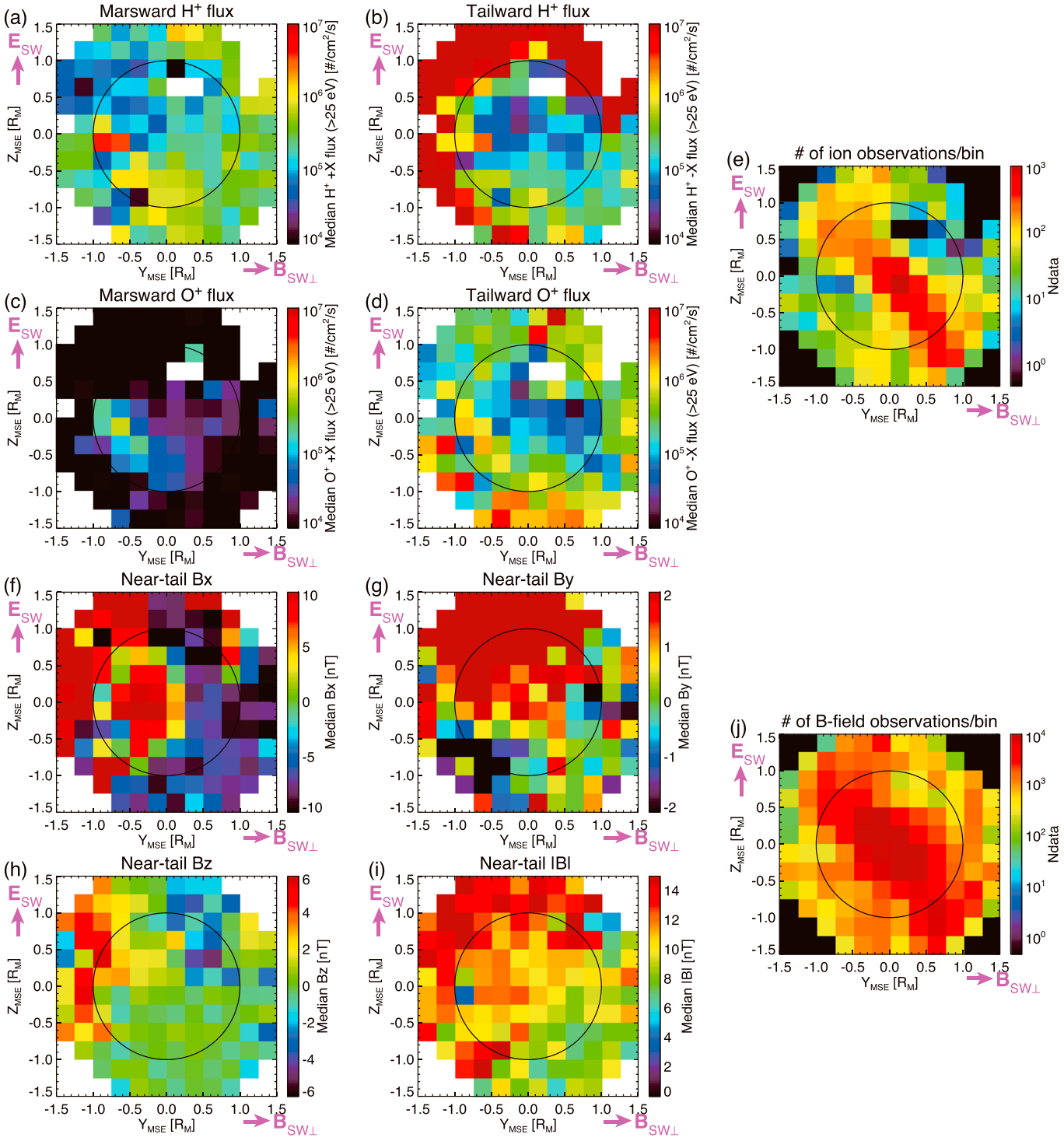

Figure 2. Y_{MSE}-Z_{MSE} distributions of ion flux and magnetic field in the near-Mars magnetotail ($\rho_{MSO} < 1.5R_M$ and $-1.5R_M < X_{MSO} < -1R_M$) derived from data taken from 1 December 2014 to 28 February 2015. (a) Marsward and (b) tailward protons above 25 eV; (c) Marsward and (d) tailward oxygen ions above 25 eV; (e) number of ion observations in each bin; (f) *X*, (g) *Y*, and (h) *Z* components; (i) intensity of the magnetic field in the MSE frame, and (j) number of 1 s magnetic field observations in each bin.

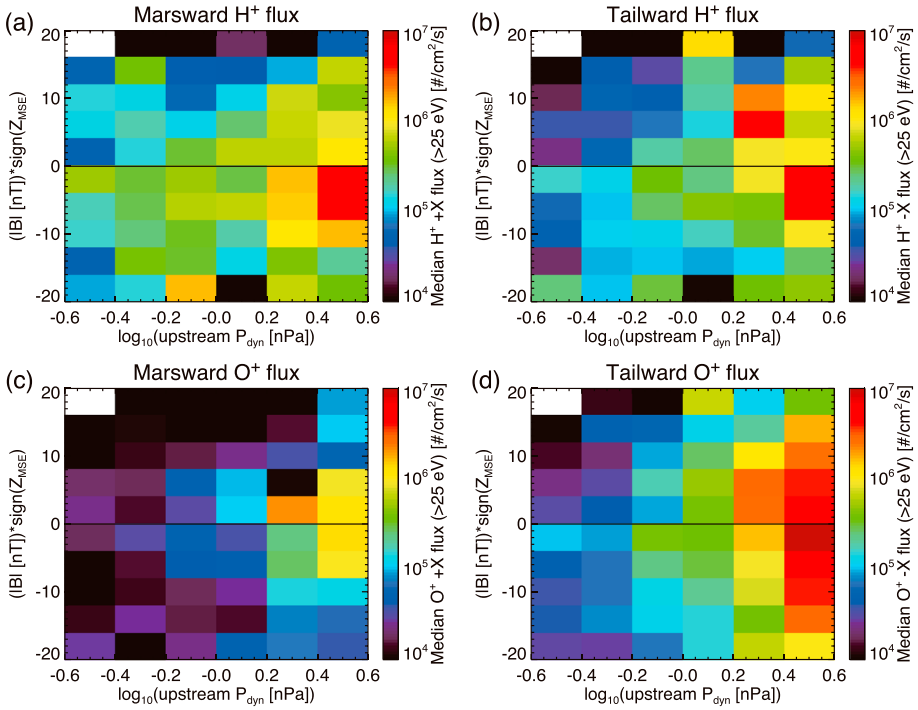

Figure 3. Median distributions of ion flux in the near-Mars wake ($\rho_{MSO} < 1R_M$ and $-1.5R_M < X_{MSO} < -1R_M$) as a function of local magnetic field intensity with the sign of Z_{MSE} and upstream dynamic pressure for (a) Marsward and (b) tailward protons above 25 eV and (c) Marsward and (d) tailward oxygen ions above 25 eV.

We first investigate the solar wind electric field control of the near-Mars magnetotail ($\rho_{MSO} < 1.5R_M$ and $-1.5R_M < X_{MSO} < -1R_M$) by sorting data into the Mars Solar Electric (MSE) frame; i.e., $+X$ points from Mars toward $-\mathbf{V}_{SW}$, $+Z$ is parallel to $\mathbf{E}_{SW} = -\mathbf{V}_{SW} \times \mathbf{B}_{SW}$, and Y completes the orthogonal coordinate set. Figures 2a–2d and 2f–2i show Y_{MSE}-Z_{MSE} distributions of directional ion fluxes and magnetic field components, respectively. Median values in each bin are used to present the typical state of the near-Mars magnetotail. The data density distributions for the ion and magnetic field observations are shown in Figures 2e and 2j. We note that the $Y_{MSE} < 0$, $Z_{MSE} > 0$ quadrant and the $Y_{MSE} > 0$, $Z_{MSE} < 0$ quadrant are better sampled compared to the other two quadrants because of the typically horizontal IMF orientation and inclined MAVEN orbits. This MAVEN data set provides sufficient numbers of observations in the $\pm E$ hemispheres for the purpose of studying hemispheric asymmetry of the near-Mars magnetotail.

We observe the asymmetric distribution of Marsward protons with larger flux in the $Z_{MSE} < 0$ ($-E$) wake compared to the $Z_{MSE} > 0$ ($+E$) hemisphere (Figure 2a). The tailward proton flux inside the wake (Figure 2b) is generally smaller than the Marsward flux. We observe the small Marsward flux of oxygen ions mainly in the $-E$ hemisphere (Figure 2c). The tailward oxygen ion flux (Figure 2d) dominates over the Marsward flux throughout the tail. We see some asymmetry in the tailward oxygen ions as well, e.g., the broadly distributed, moderate flux in the $-E$ hemisphere and the narrow and strong flux in the $+E$ tail (at Y_{MSE} ~0–0.5 R_M and Z_{MSE} ~1–1.5 R_M). The $\pm E$ asymmetry of tailward oxygen ions becomes more prominent in farther downtail regions [*Dong et al.*, 2015].

The magnetic field structure in the near-Mars magnetotail also exhibits clear asymmetry relative to the upstream solar wind electric field. Figure 2f demonstrates the expected two-lobe structure: the positive B_x on the $Y_{MSE} < 0$ side and negative B_x on the $Y_{MSE} > 0$ side. In the B_y panel (Figure 2g), we observe positive B_y in the $+E$ hemisphere, while B_y has smaller, even negative, values in the $-E$ hemisphere. The B_z distribution (Figure 2h) shows the upward field (positive B_z) in the $Y_{MSE} < 0$, $Z_{MSE} > 0$ quadrant; downward field (negative B_z) in the $Y_{MSE} > 0$, $Z_{MSE} > 0$ quadrant; and mostly horizontal field ($B_z \sim 0$) in the $-E$ hemisphere. The magnetic field intensity is generally stronger in the $+E$ hemisphere compared to the $-E$ hemisphere (Figure 2i). Overall, the $+E$ hemisphere is characterized by stronger magnetic fields with significant $+B_y$ and $\pm B_z$ components, while the field lines are more tightly wrapped around Mars (i.e., B_y reversal) in the $-E$ hemisphere.

In addition to the $\pm E$ asymmetry, the observed ion fluxes are well organized by the local magnetic field intensity and upstream dynamic pressure. Figures 3a–3d show medians of Marsward and tailward fluxes of protons and oxygen ions in the near-Mars wake region ($\rho_{MSO} < 1R_M$ and $-1.5R_M < X_{MSO} < -1R_M$) as a function of local magnetic field intensity and upstream dynamic pressure. The local magnetic field intensity with the sign of Z_{MSE} (y axis) provides a measure of the two main regions in the magnetotail for the $\pm E$ hemispheres: the strong-field tail lobes formed by the draped IMF and the weak-field plasma sheet sandwiched between the oppositely directed lobe fields. We observe generally large ion fluxes in weak magnetic fields as expected in the hot plasma sheet. The ion fluxes are also sorted by the upstream dynamic pressure (x axis), showing larger fluxes in higher dynamic pressure conditions. The Marsward proton flux displays clear asymmetry relative to the solar wind electric field (Figure 3a), while the other fluxes appear to be more or less symmetric in these coordinates (Figures 3b–3d). Again, we observe mostly Marsward dominant proton fluxes (Figures 3a and 3b) and tailward dominant oxygen ion fluxes (Figures 3c and 3d). Finally, our preliminary study has not yet identified any obvious effects of crustal magnetic fields on tail ion fluxes (not shown), though more detailed investigation would be necessary to fully reveal the complicated role of crustal fields in the Martian magnetosphere.

4. Discussion

The dynamic-pressure dependence of the tailward planetary ion flux (Figure 3d) is consistent with previous Mars Express observations [*Lundin et al.*, 2008], and the MAVEN observations have revealed that the fluxes of Marsward ions and tailward protons are also controlled by the upstream dynamic pressure (Figures 3a–3c). Larger ion fluxes are found in the weak magnetic field region (Figures 3a–3d), reflecting the magnetotail structure of the plasma sheet and tail lobes. These observations indicate that the significant return fluxes of plasma sheet ions are directly or indirectly controlled by the upstream solar wind condition.

Next we discuss the hemispheric asymmetry in the near-Mars magnetotail and compare them to Venus observations. We observe the enhanced Marsward proton flux and negative B_y in the $-E$ hemisphere (Figures 2a and 2g). Very similar $\pm E$ asymmetry of return ion flows and IMF draping pattern has been observed at Venus [*Zhang et al.*, 2010; *Du et al.*, 2013; *Dubinin et al.*, 2013, 2014; *Rong et al.*, 2014], suggesting the presence of common physical processes. Proposed mechanisms for production of the Venusward ion flows include inward magnetic tension and magnetic reconnection owing to the tight wrapping of field lines in the $-E$ hemisphere [*Zhang et al.*, 2012; *Dubinin et al.*, 2013]. Similar explanations seem to be applicable to Marsward ion flows in the Martian magnetotail, considering the observed field line wrapping in the $-E$ hemisphere (Figure 2g). However, we also find a striking difference between the observations at Mars and Venus: mass dependence of the net flux directions. The MAVEN observations show the net Marsward flux of protons and net tailward flux of oxygen ions in the $-E$ hemisphere (Figures 2a–2d and 3a–3d), whereas both species tend to have Venusward flows on average in the $-E$ near-Venus tail [*Dubinin et al.*, 2013]. We note that event studies at Venus show an example of only protons traveling Venusward with oxygen ions almost stagnant in the plasma sheet, and this event was interpreted as a signature of a magnetic island produced by magnetic reconnection [*Dubinin et al.*, 2012b]. It remains uncertain what makes the difference between the average states of Martian and Venusian magnetotails. We will leave detailed event analyses as well as more extended statistical studies with other parameters, including crustal field effects, to a future investigation.

Here we briefly investigate the relations between the ion flows and local magnetic field configurations. Figure 4 shows mean velocity vectors of suprathermal protons and oxygen ions and local magnetic fields on the X_{MSE}-Y_{MSE} plane in the $-0.75R_M < Z_{MSE} < -0.25R_M$ and $\rho_{MSO} < 1R_M$ ranges. In this spatial range, the Marsward proton flows are frequently observed (Figure 4a), mostly tailward oxygen ion flows are seen (Figure 4b), and the magnetic field vectors exhibit very complicated field configurations (Figure 4c). We note that the Marsward proton flows do not necessarily coincide with the local negative $B_{y,MSE}$ values, suggesting that the relations between ion flow directions and local magnetic field structures may not be simple.

The planetward ions in the magnetotail can be found in a number of simulation results for Mars and Venus [*Ma et al.*, 2002, 2004; *Terada et al.*, 2002, 2004; *Bößwetter et al.*, 2004, 2007, 2010; *Fang et al.*, 2008; *Najib et al.*, 2011; *Curry et al.*, 2013; *Jarvinen et al.*, 2013]. Most model studies have focused on planetary ion escape and have not yet investigated the details of the return fluxes such as planetward acceleration processes and

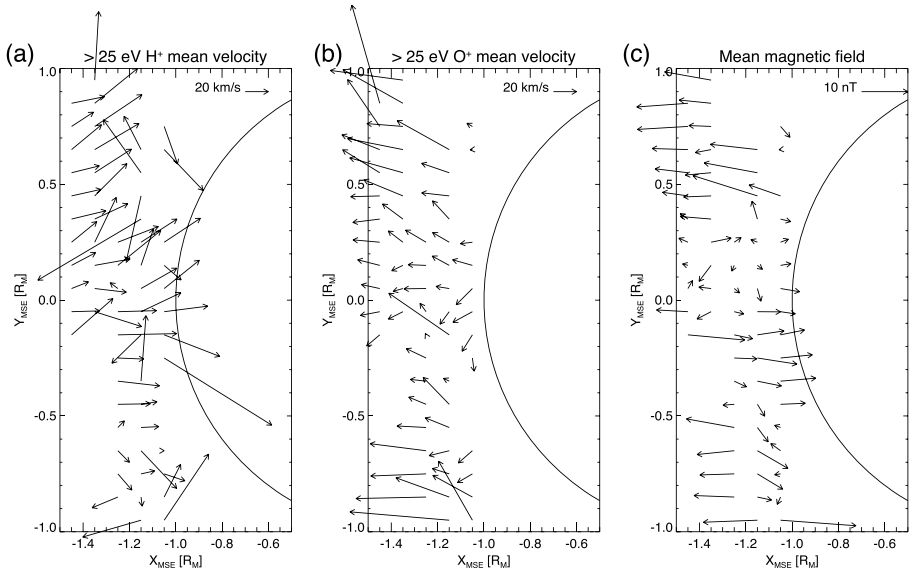

Figure 4. X_{MSE}-Y_{MSE} projections of >25 eV (a) proton and (b) oxygen ion velocity vectors and of (c) local magnetic field vectors within $-0.75R_M < Z_{MSE} < -0.25R_M$ and $\rho_{MSO} < 1R_M$.

their dependence on ion species and Z_{MSE}. Reinvestigation of these model results as well as new simulation runs specifically focusing on this topic will provide useful information for interpretation of the observed planetward ions associated with the asymmetric magnetic field draping pattern.

5. Conclusions

MAVEN observations illustrate the coexistence of hot magnetosheath protons, cold planetary protons, cold planetary heavy ions, and energetic heavy pickup ions in the near-Mars magnetotail. The suprathermal (>25 eV) protons and oxygen ions travel in different directions, suggesting their kinetic/multifluid nature. The statistical results show that upstream solar wind and magnetic field conditions control the hot ion fluxes in the near-Mars ($-1.5R_M < X_{MSO} < -1R_M$) magnetotail. Both Marsward and tailward ion fluxes are well organized by the solar wind dynamic pressure and local magnetic field intensity. The spatial distributions of the Marsward protons and local magnetic field in the magnetotail exhibit clear asymmetry relative to the solar wind motional electric field. We observe larger fluxes of Marsward protons and field line wrapping in the $-E$ hemisphere as observed at Venus. However, unlike at Venus, where both protons and oxygen ions tend to have Venusward velocities in the $-E$ hemisphere, MAVEN observations show the net Marsward flux of protons but net tailward flux of oxygen ions on average. The details of processes which produce such Marsward proton fluxes in the presence of tailward traveling oxygen ions remain unclear.

Acknowledgments

The authors wish to acknowledge great support from the team members of the MAVEN mission. This work was partially supported by the CNES for the part based on observations with the SWEA instrument embarked on MAVEN. MAVEN data are publicly available through the Planetary Data System.

The Editor thanks Andrey Fedorov and an anonymous reviewer for their assistance in evaluating this paper.

References

Barabash, S., et al. (2007), The loss of ions from Venus through the plasma wake, *Nature*, *450*(7170), 650–653, doi:10.1038/nature06434.

Bößwetter, A., T. Bagdonat, U. Motschmann, and K. Sauer (2004), Plasma boundaries at Mars: A 3-D simulation study, *Ann. Geophys.*, *22*(12), 4363–4379, doi:10.5194/angeo-22-4363-2004.

Bößwetter, A., et al. (2007), Comparison of plasma data from ASPERA-3/Mars-Express with a 3-D hybrid simulation, *Ann. Geophys.*, *25*(8), 1851–1864, doi:10.5194/angeo-25-1851-2007.

Bößwetter, A., H. Lammer, Y. Kulikov, U. Motschmann, and S. Simon (2010), Non-thermal water loss of the early Mars: 3D multi-ion hybrid simulations, *Planet. Space Sci.*, *58*(14–15), 2031–2043, doi:10.1016/j.pss.2010.10.003.

Brain, D., et al. (2010), A comparison of global models for the solar wind interaction with Mars, *Icarus*, *206*(1), 139–151, doi:10.1016/j.icarus.2009.06.030, solar Wind Interactions with Mars.

Connerney, J., J. Espley, P. Lawton, S. Murphy, J. Odom, R. Oliversen, and D. Sheppard (2015), The MAVEN magnetic field investigation, *Space Sci. Rev.*,1–35, doi:10.1007/s11214-015-0169-4.

Curry, S. M., M. Liemohn, X. Fang, Y. Ma, and J. Espley (2013), The influence of production mechanisms on pick-up ion loss at Mars, *J. Geophys. Res. Space Physics*, *118*, 554–569, doi:10.1029/2012JA017665.

Dong, Y., X. Fang, D. A. Brain, J. P. McFadden, J. S. Halekas, J. E. Connerney, S. M. Curry, Y. Harada, J. G. Luhmann, and B. M. Jakosky (2015), Strong plume fluxes at Mars observed by MAVEN: An important planetary ion escape channel, *Geophys. Res. Lett.*, *42*, doi:10.1002/2015GL065346.

Du, J., C. Wang, T. L. Zhang, and E. Kallio (2013), Asymmetries of the magnetic field line draping shape around Venus, *J. Geophys. Res. Space Physics*, *118*, 6915–6920, doi:10.1002/2013JA019127.
Dubinin, E., M. Fraenz, A. Fedorov, R. Lundin, N. Edberg, F. Duru, and O. Vaisberg (2012a), Ion energization and escape on Mars and Venus, *Space Sci. Rev.*, *162*, 173–211, doi:10.1007/978-1-4614-3290-6_6.
Dubinin, E., M. Fraenz, J. Woch, T. L. Zhang, J. Wei, A. Fedorov, S. Barabash, and R. Lundin (2012b), Bursty escape fluxes in plasma sheets of Mars and Venus, *Geophys. Res. Lett.*, *39*, L01104, doi:10.1029/2011GL049883.
Dubinin, E., M. Fraenz, T. L. Zhang, J. Woch, Y. Wei, A. Fedorov, S. Barabash, and R. Lundin (2013), Plasma in the near Venus tail: Venus Express observations, *J. Geophys. Res. Space Physics*, *118*, 7624–7634, doi:10.1002/2013JA019164.
Dubinin, E., M. Fraenz, T. L. Zhang, J. Woch, and Y. Wei (2014), Magnetic fields in the Venus ionosphere: Dependence on the IMF direction—Venus express observations, *J. Geophys. Res. Space Physics*, *119*, 7587–7600, doi:10.1002/2014JA020195.
Ergun, R. E., L. Andersson, W. K. Peterson, D. Brain, G. T. Delory, D. L. Mitchell, R. P. Lin, and A. W. Yau (2006), Role of plasma waves in Mars' atmospheric loss, *Geophys. Res. Lett.*, *33*, L14103, doi:10.1029/2006GL025785.
Fang, X., M. W. Liemohn, A. F. Nagy, Y. Ma, D. L. De Zeeuw, J. U. Kozyra, and T. H. Zurbuchen (2008), Pickup oxygen ion velocity space and spatial distribution around Mars, *J. Geophys. Res.*, *113*, A02210, doi:10.1029/2007JA012736.
Fedorov, A., et al. (2008), Comparative analysis of Venus and Mars magnetotails, *Planet. Space Sci.*, *56*(6), 812–817, doi:10.1016/j.pss.2007.12.012. Mars Express/Venus Express.
Halekas, J., E. Taylor, G. Dalton, G. Johnson, D. Curtis, J. McFadden, D. Mitchell, R. Lin, and B. Jakosky (2013), The solar wind ion analyzer for MAVEN, *Space Sci. Rev.*,1–27, doi:10.1007/s11214-013-0029-z.
Halekas, J. S., et al. (2015), MAVEN Observations of Solar Wind Hydrogen Deposition in the Atmosphere of Mars, *Geophys. Res. Lett.*, *42*, doi:10.1002/2015GL064693, in press.
Jakosky, B. M., et al. (2015), The Mars Atmosphere and Volatile EvolutioN (MAVEN) mission, *Space Sci. Rev.*,1–46, doi:10.1007/s11214-015-0139-x.
Jarvinen, R., E. Kallio, and S. Dyadechkin (2013), Hemispheric asymmetries of the Venus plasma environment, *J. Geophys. Res. Space Physics*, *118*, 4551–4563, doi:10.1002/jgra.50387.
Lundin, R. (2011), Ion acceleration and outflow from Mars and Venus: An overview, *Space Sci. Rev.*, *162*(1–4), 309–334, doi:10.1007/s11214-011-9811-y.
Lundin, R., S. Barabash, A. Fedorov, M. Holmström, H. Nilsson, J.-A. Sauvaud, and M. Yamauchi (2008), Solar forcing and planetary ion escape from Mars, *Geophys. Res. Lett.*, *35*, L09203, doi:10.1029/2007GL032884.
Ma, Y., A. F. Nagy, K. C. Hansen, D. L. DeZeeuw, T. I. Gombosi, and K. G. Powell (2002), Three-dimensional multispecies MHD studies of the solar wind interaction with Mars in the presence of crustal fields, *J. Geophys. Res.*, *107*(A10), 1282, doi:10.1029/2002JA009293.
Ma, Y., A. F. Nagy, I. V. Sokolov, and K. C. Hansen (2004), Three-dimensional, multispecies, high spatial resolution MHD studies of the solar wind interaction with Mars, *J. Geophys. Res.*, *109*, A07211, doi:10.1029/2003JA010367.
McFadden, J., et al. (2014), The MAVEN Suprathermal and thermal Ion Composition (STATIC) instrument, *Space Sci. Rev.*, in press.
Mitchell, D. L., et al. (2014), The MAVEN Solar Wind Electron Analyzer (SWEA), *Space Sci. Rev.*, in press.
Nagy, A., et al. (2004), The plasma environment of Mars, *Space Sci. Rev.*, *111*(1–2), 33–114, doi:10.1023/B:SPAC.0000032718.47512.92.
Najib, D., A. F. Nagy, G. Tóth, and Y. Ma (2011), Three-dimensional, multifluid, high spatial resolution MHD model studies of the solar wind interaction with Mars, *J. Geophys. Res.*, *116*, A05204, doi:10.1029/2010JA016272.
Rong, Z. J., S. Barabash, Y. Futaana, G. Stenberg, T. L. Zhang, W. X. Wan, Y. Wei, X.-D. Wang, L. H. Chai, and J. Zhong (2014), Morphology of magnetic field in near-Venus magnetotail: Venus express observations, *J. Geophys. Res. Space Physics*, *119*, 8838–8847, doi:10.1002/2014JA020461.
Slavin, J. A., D. S. Intriligator, and E. J. Smith (1989), Pioneer Venus Orbiter magnetic field and plasma observations in the Venus magnetotail, *J. Geophys. Res.*, *94*(A3), 2383–2398, doi:10.1029/JA094iA03p02383.
Terada, N., S. Machida, and H. Shinagawa (2002), Global hybrid simulation of the Kelvin-Helmholtz instability at the Venus ionopause, *J. Geophys. Res.*, *107*(A12), 1471, doi:10.1029/2001JA009224.
Terada, N., H. Shinagawa, and S. Machida (2004), Global hybrid model of the solar wind interaction with the Venus ionosphere: Ion escape processes, *Adv. Space Res.*, *33*(2), 161–166, doi:10.1016/j.asr.2003.05.011, planetary Atmospheres, Ionospheres and Plasma Interactions.
Trotignon, J., C. Mazelle, C. Bertucci, and M. Acuña (2006), Martian shock and magnetic pile-up boundary positions and shapes determined from the Phobos 2 and Mars global surveyor data sets, *Planet. Space Sci.*, *54*(4), 357–369, doi:10.1016/j.pss.2006.01.003.
Zhang, T. L., W. Baumjohann, J. Du, R. Nakamura, R. Jarvinen, E. Kallio, A. M. Du, M. Balikhin, J. G. Luhmann, and C. T. Russell (2010), Hemispheric asymmetry of the magnetic field wrapping pattern in the Venusian magnetotail, *Geophys. Res. Lett.*, *37*, L14202, doi:10.1029/2010GL044020.
Zhang, T. L., et al. (2012), Magnetic reconnection in the near Venusian magnetotail, *Science*, *336*(6081), 567–570, doi:10.1126/science.1217013.